Eur. Phys. J. C 9, 503–510 (1999)
Digital Object Identifier (DOI) 10.1007/s100529900042

THE EUROPEAN PHYSICAL JOURNAL C

Strong and electromagnetic decays of excited heavy mesons

A. Hiorth Örsland, H. Högaasen

Department of Physics, University of Oslo, P.O. Box 1048 Blindern, N-0316 Oslo, Norway

Received: 19 January 1999 / Published online: 18 June 1999

Abstract. We discuss a model for heavy mesons where the light quark (u or d) moves in the colour-electric field from a heavy quark (c or b) placed in the center of a bag. We calculate energy spectra for pionic and photonic transitions from excited states. The transition amplitudes and the branching ratios between electromagnetic and pionic transitions compare favorably with the limited amount of known experimental data.

1 Introduction

Heavy-quark spectroscopy is a very interesting and rewarding subject for study. The discovery of charmonium definitively swept away all doubts the physics community had about the existence of quarks as the fundamental building blocks of hadrons.

Mesons consisting of one heavy and one light quark (denoted $Q\bar{q}$) are a further excellent subject on which to test our ideas about strong interactions. These mesons are, in a way, the hydrogen atoms of quark physics. As the mass of the heavy quark increases, its motion becomes gradually less and less important, and the physical properties of the heavy–light meson, $Q\bar{q}$, are more and more determined by the dynamics of the light quark.

The discovery of the heavy-quark symmetries by Isgur and Wise [1,2] and the creation of a heavy-quark effective theory from QCD [3–5] have been extremely important for the analysis of the physics of heavy hadrons [6].

Ideally, one would like to compute the couplings in the baryon and meson Lagrangian from QCD; in time, this should be provided by lattice QCD calculations. In the meantime, model calculations can be useful, and one might hope that these give us some physical insight for the long-distance behavior of quark interaction.

2 The model

There are many models used in quark physics; we have chosen a variant of the MIT bag model that was created by W. Wilcox, O. V. Maxwell and K. A. Milton [7] (WWM), at a time when there was little information about excited systems made of one heavy and one light quark.

The model makes for a nice theoretical laboratory; it lends itself to analytical calculations, and seems to give results that are not too far from experimental results. In particular, it seems to work well for calculations of the Isgur–Wise function [8] and to represent an improvement over the results from the MIT bag model [9]. In the WMM model, the heavy quark is placed in the center of the bag, and the light quark moves within the colour-electromagnetic field set up by the heavy quark. The Hamiltonian for the light quark is then

$$H = H_0 + H_I \tag{1}$$

where

$$H_0 = \boldsymbol{\alpha} \cdot \boldsymbol{p} + \beta m + g \boldsymbol{t}_{\mathrm{l}a} V^a,\ t_a \equiv \frac{\lambda_a}{2}\ a = 1, \ldots, 8 \tag{2}$$

and

$$H_I = -g t_{\mathrm{l}a} \boldsymbol{\alpha} \cdot \boldsymbol{A}^a. \tag{3}$$

t_a represents a generator of the $\mathrm{SU}(3)_C$ colour group. The index l (h) refers to the light (heavy) quark. We have used $A^\mu_a = (V_a, \boldsymbol{A}_a)$ and the usual notation $\alpha_i = \gamma^0\gamma_i$ and $\beta = \gamma^0$, where the γs are the Dirac matrices, and λ_a the Gellman matrices. V_a and $\boldsymbol{A_a}$ are the colour-electric potentials and vector fields respectively produced by the heavy quark.

As gluon self-couplings are neglected and the heavy quark is treated as point-like, the potentials have a Coulomb-like form:

$$V_a = \frac{g t_{\mathrm{h}a}}{4\pi r}. \tag{4}$$

Substituting these potentials into equation (2) gives us:

$$H_0 = \boldsymbol{\alpha} \cdot \boldsymbol{p} + \beta m + \frac{g^2 t^a_{\mathrm{l}} t_{\mathrm{h}a}}{4\pi r}. \tag{5}$$

Using the constraint that the meson is a colour singlet, that is, $t^a_{\mathrm{l}} t_{\mathrm{h}a} = -4/3$, the Hamiltonian of the light quark in the meson rest frame is then simply

$$H_0 = \boldsymbol{\alpha} \cdot \boldsymbol{p} + \beta m - \frac{\xi}{r}, \tag{6}$$

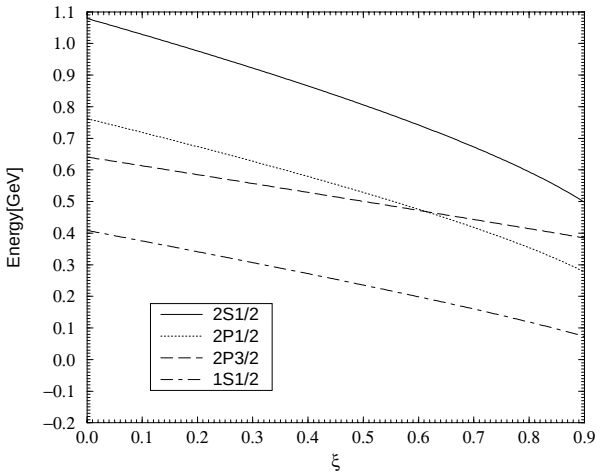

Fig. 1. Energy levels inside a bag with radius $R = 5\text{GeV}^{-1}$

where $\xi = (4/3)\alpha_s = (4/3)(g^2/4\pi)$.

The four-component wave function $\psi(r)$ of the light quark (ignoring H_I) is therefore the well-known solution for the relativistic Coulomb problem. We shall use the notation

$$\psi(r) = \begin{pmatrix} g(r)\chi^\mu_\kappa \\ \mathrm{i}f(r)\chi^\mu_{-\kappa} \end{pmatrix}, \tag{7}$$

where χ^μ_κ is the two-component spinor describing the angular part of the wave function.

The energy of the confined light quark is determined by the Bogolioubov–MIT boundary condition [10,11] which in the rest frame of the meson, takes the form $-\mathrm{i}(\hat{\boldsymbol{r}} \times \boldsymbol{\gamma})\psi = \psi$. Substituting equation (7) into this equation and using the following property $(\boldsymbol{\sigma} \times \hat{\boldsymbol{r}})\chi^\mu_\kappa = -\chi^\mu_{-\kappa}$, we get:

$$f(R) + g(R) = 0, \tag{8}$$

where R is the radius of the spherical bag. The confinement of the light quark, presumably originating from the gluonic self-couplings, is now taken care of by (8) and the surface conditions

$$\hat{\boldsymbol{r}} \times \boldsymbol{E}^a = 0 \tag{9}$$

$$\hat{\boldsymbol{r}} \times \boldsymbol{B}^a = 0. \tag{10}$$

The vector fields $\boldsymbol{A}_a$ that are set up by the heavy quark and fulfill the boundary conditions (10), are

$$\boldsymbol{A}_a = \frac{1}{4\pi}\left(\frac{\boldsymbol{m}_a \times \hat{\boldsymbol{r}}}{r^3} + \frac{\boldsymbol{m}_a \times \hat{\boldsymbol{r}}}{2R^3}\right), \tag{11}$$

where $\boldsymbol{m}_a$ are the colour-magnetic moments of the heavy quark:

$$\boldsymbol{m}_a = \frac{g t_{\mathrm{h}a}}{M_{\mathrm{h}}}\boldsymbol{S}. \tag{12}$$

M_{h} is the mass of the heavy quark and $\boldsymbol{S}$ its spin operator. H_I can now be written:

$$H_I = \frac{\alpha_s t_{\mathrm{l}a} t_{\mathrm{h}}{}^a}{M_{\mathrm{h}}}\boldsymbol{S} \cdot (\boldsymbol{\alpha} \times \hat{\boldsymbol{r}})\left(\frac{1}{r^2} + \frac{r}{2R^3}\right) \tag{13}$$

The contribution of H_I to the energy is calculated perturbatively, and the hyperfine splitting energy to first order in α_s is

$$E^1_I = \frac{8}{3}\frac{\alpha_s}{M}\frac{\kappa}{4\kappa^2 - 1}\left(F(F+1) - J(J+1) - \frac{3}{4}\right) \times \frac{1}{N}\int_0^R \mathrm{d}r\left(2 + \frac{r^3}{R^3}\right) f(r)^* g(r). \tag{14}$$

N is the normalization of the wave function, $N \equiv \int_0^R \mathrm{d}r r^2 (|f(r)|^2 + |g(r)|^2)$. Here F is the total angular momentum of the mesonic system and J is the light-quark (total) angular momentum. From (14), we see if $M_{\mathrm{h}} \to \infty$ then $E^1_I \to 0$; this is the heavy-quark limit.

The mass function for a heavy meson described in our model will be:

$$M = M(R) = E_{\mathrm{Vol}} + E_{\mathrm{Zero}} + m_Q + E_q, \tag{15}$$

where $E_{\mathrm{Vol}} = (4\pi/3)BR^3$ is the energy needed to create a bag in a vacuum, E_{Zero} is the zero-point energy proportional to $1/R$, m_Q is the heavy-quark mass, and E_q is the light-quark energy $E_q \equiv \sqrt{p_q^2 + m_q^2} + E^1_I$, where $E^1_I$is the hyperfine splitting energy to first order given in (14). From (15), we observe that if the radii of two mesons (with the same flavour of the heavy quark) are kept constant, then the mass difference between them is given by the following formula:

$$\Delta M = E_q(nL_J) - E_q(n'L'_{J'}). \tag{16}$$

This means that if the radii of two mesons do not differ too much, then the difference between the energy levels is directly related to the mass difference of the two mesons.

It is of interest first to see how the energy levels of the meson are ordered in the heavy-quark limit when the colour-electric central potential increases, these are shown in Fig. 1.

As we can see, an increase in the central field from the special case where the light quark moves freely in the bag reduces the masses of the P states, and even makes them cross. The odd-parity states, however, stay roughly half-way between the ground state and the first excited S state. This will lead to some difficulties when we try to fit the spectra of heavy- meson states.

The breaking of the heavy-quark limit is given by the spin–spin interaction and, in our model, by the term E^1_I, as given (14). It should be noted that this term is dependent on α_s, which determines the strength of the central four-vector potential the light quark moves in. In this respect, our model is more constraining than most models where the interquark central potential is unrelated to the strength of the spin–spin and spin–orbit interaction.

In Fig. 2, we have plotted the energy levels for the light quark in the case where $M = m_b$ for constant R. In this graph, we have also plotted the heavy-quark limit; the energy level above the heavy-quark limit is for each pair of states, where the spin of the light quark and the heavy quark couples to $S = 1$, and the level below is for the case where the spins couple to $S = 0$.

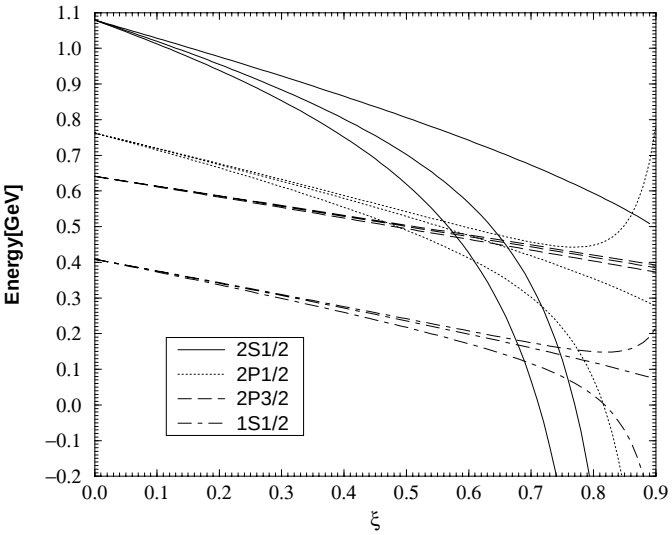

Fig. 2. The energy of a (massless) light quark inside a Coulomb bag with radius $R = 5\text{GeV}^{-1}$ and the mass of a heavy quark $m_b = 4730$ MeV

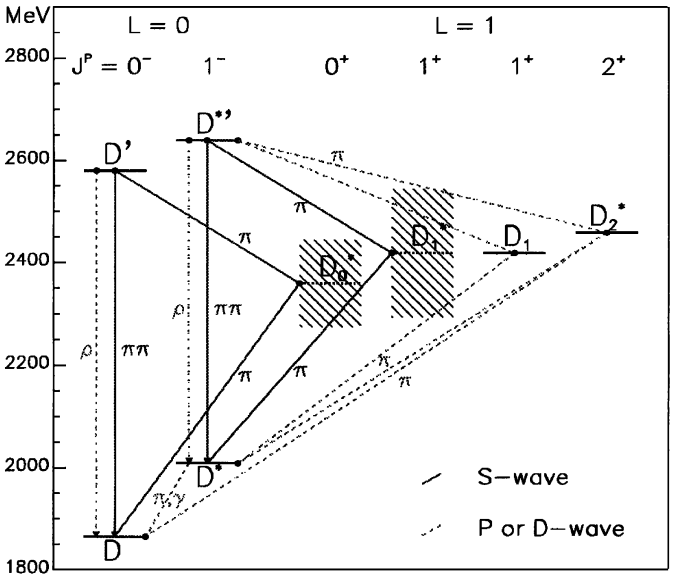

Fig. 3. D-meson spectra and transition lines

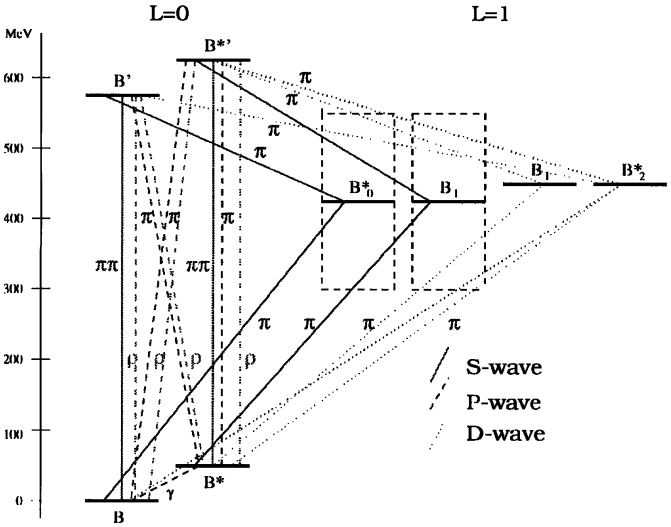

Fig. 4. B-meson spectra and transition lines

We see that for a given heavy-quark multiplet, the induced splitting of formerly degenerate states with the same angular momentum, J for the light quark, but with different angular momentums, F, for the meson, is a highly nonlinear function of α_s. Only for α_s smaller than 0.2 is it a reasonable approximation to take the hyperfine splitting as a linear function of α_s (as it is in the nonrelativistic quark model treatment).

From Fig. 2 we also note that the hyperfine splitting (for finite ξ) increases as light-quark excitations increase. This is quite opposite from the situation for the hydrogen atom, and is a reflection of the bag model's abrupt confinement.

For the charm sector, it is reasonable only for the two lowest states to calculate the hyperfine splitting perturbatively, this is because of the much smaller mass of the c quark.

3 The mass function for heavy mesons

In the previous section we looked at the qualitative features of the spectra of heavy mesons. Now we will try to reproduce the quantitatively measured masses. In Figs. 3 and 4 we have shown the observed spectra of the D and B mesons. The mass formula for heavy mesons in our model is:

$$M = \frac{4}{3}BR^3 + \frac{C}{R} + m_Q + \sqrt{{p_q}^2 + m_q} + \frac{8}{3}\frac{\alpha_s}{M}\frac{\kappa}{4\kappa^2 - 1} \times \left(F(F+1) - j(j+1) - \frac{3}{4}\right)\mathcal{I}, \tag{17}$$

where $\mathcal{I}$ is an integral over the radial wave functions

$$\mathcal{I} = \frac{1}{N}\int_0^R \mathrm{d}r \left(2 + \frac{r^3}{R^3}\right) f(r)^* g(r). \tag{18}$$

When calculating the Coulomb potential in classical electrodynamics, it is common to choose

$$V(r) = 0 \qquad \text{for} \qquad r \longrightarrow \infty. \tag{19}$$

Inspired by this, we adjust the potential inside the bag to be zero at the surface of the bag [12]:

$$V(r) = -\frac{\xi}{r} \longrightarrow -\xi\left(\frac{1}{r} - \frac{1}{R}\right). \tag{20}$$

Now the value of the potential at the bag surface will be zero, independent of the radii of the different mesons. Because of this transformation, the light quark gets a contribution ξ/R to the energy.

The second term, C/R, in (17) is believed to represent the zero-point energy in the bag. When one quantizes a radiation field, there will always be an infinite zero-point

Table 1. The parameters are $B^{1/4} = 161\,\mathrm{MeV}, \xi = 0.538$ ($\alpha_s = 0.404$), $m_u = m_d = 10\,\mathrm{MeV}$, and $m_b = 4627\,\mathrm{MeV}$; $e_q = e_Q = -1/3$ for d and b quarks and $e_q = e_Q = 2/3$ for u and c quarks

	Experimental data	Theoretical results				
	Mass (MeV)	Mass (MeV)	F^P	State	Radius (GeV^{-1})	μ_m/μ_N
B	5279.4 ± 2.2 [15]	5279	0^-	$1S_{1/2}$	3.94	0
B^*	5324.9 ± 1.8 [15]	5325	1^-	$1S_{1/2}$	3.94	$1.52e_q + 0.203e_Q$
B_0	not observed	5592	0^+	$2P_{1/2}$	4.50	0
B_1	not observed	5671	1^+	$2P_{1/2}$	4.50	$0.625e_q + 0.203e_Q$
B_1	5725 [16]	5623	1^+	$2P_{3/2}$	4.47	$1.93e_q + 0.101e_Q$
B_2	5737 [16]	5637	2^+	$2P_{3/2}$	4.47	$2.33e_q + 0.203e_Q$
B'	5859 [17]	5859	0^-	$2S_{1/2}$	4.90	0
B'^*	not observed	5967	1^-	$2S_{1/2}$	4.90	$0.597e_q + 0.203e_Q$

energy term, but since physical quantities are often energy differences, the zero-point energy falls out. However, when the quantization is carried out in a finite cavity, as in our model, there will be additional pieces of the zero-point energy that depend on the size of the cavity. This is represented by the term C/R. The constant C can be calculated if we believe that the zero-point energy gives rise to the Casimir energy. The Casimir energy inside a perfectly uncharged spherical shell has been calculated by K. A. Milton, L. L. DeRaad, Jr., and J. Schwinger [13]. They obtained the value $E = 0.09235/(2R)$. To find the value in our model, we simply have to multiply the value by eight, because there are eight gluonic radiation fields:

$$C \simeq 0.37. \tag{21}$$

We have determined the masses by minimizing the mass function by the relation:

$$\frac{\partial M}{\partial R} = 0. \tag{22}$$

The integral in (18) turns out to be

$$\frac{1}{m_Q R^2}. \tag{23}$$

Since $p_q \sim 1/R$, it is clear that when $R \longrightarrow 0$, $\mathcal{I}$ will dominate. If the factor in front of the hyperfine splitting is negative, (17) will, for some choice of the parameters, have no finite minima. When the radius becomes small, we cannot neglect the repulsion of the heavy quark, and thus the model becomes meaningless. This is a well-known problem, and the usual way of dealing with it is to argue that the divergence will disappear when we calculate higher-order corrections. The procedure, then, is to minimize the energy with respect to R *before* adding the hyperfine term [14]. In our model, states with same J and L will then have equal radii.

4 Heavy meson masses

First of all, we have to determine the parameters in the model. There are four parameters the strong coupling constant (α_s), the bag constant (B), the heavy-quark mass (m_Q) and the light-quark mass (m_q). There are, of course, many ways of determining the parameters; we have chosen to look at the B mesons. We determine α_s, B, m_b from the observed masses of the B, B^* and B' mesons, and since the u and d quark have a small mass, we have assigned to them a (rather unimportant) mass of 10 MeV. The calculated results are shown in Table 1

In Table 1, there are only given uncertainties for the $1S_{1/2}$ states. This is because the values of the masses for the $2P_{3/2}$ and the lowest $2S_{1/2}$ states were found in [16] and [17] as a fit to the experimental data, and it is not quite clear how to put errors to these numbers.

Unfortunately we see that the calculated masses for the B_1 and B_2 mesons are almost exactly 100 MeV below the experimental values. However, we see that the splitting between the two $P_{3/2}$ mesons is quite well described. One may wonder if there is another set of parameters that will give us a good fit to all the experimental masses listed in Table 1. We believe that this is not so. The parameter in the system which has most influence on the spectra is ξ. In Fig. 1, we plotted the energy levels for ξ between 0 and 0.9. The main problem is that the P states do not move much in the direction of the $2S_{1/2}$ state when ξ increases. The boundary condition (8) clearly gives a wrong level splitting. A hope for the model would be that the state we used as B' is not the right one. If we used the B_1 and B_2 states (together with B and B^*) as a normalization, the resulting B' would have a mass around 6020 MeV.

Now we have the value for the strong coupling, the bag constant, and the b-quark mass. In order to calculate the D- and B_s-meson masses, we have to find the c- and s-quark masses. This is done by demanding that:

$$m(D_{\mathrm{Exp}}) - m(D_{\mathrm{Theor}}) \approx m(D^*_{\mathrm{Theor}}) - m(D^*_{\mathrm{Exp}}) \tag{24}$$

and the s-quark mass by demanding that:

$$m(B_{s\,\mathrm{Exp}}) - m(B_{s\,\mathrm{Theor}}) \approx m(B^*_{s\,\mathrm{Theor}}) - m(B^*_{s\,\mathrm{Exp}}). \tag{25}$$

The results are listed in Table 2.

Table 2. The parameters are $B^{1/4} = 161\,\mathrm{MeV}, \xi = 0.538$ ($\alpha_s = 0.404$), $m_b = 4627\,\mathrm{MeV}, m_c = 1294$ MeV, and $m_s = 231$ MeV; $e_q = e_Q = -1/3$ for d and b quarks and $e_q = e_Q = 2/3$ for u and c quarks

	Experimental data	Theoretical results				
	Mass (MeV)	Mass (MeV)	F^P	State	Radius (GeV^{-1})	μ_m/μ_N
D	1866.8 ± 1.1 [15]	1854	0^-	$1S_{1/2}$	3.94	0
D^*	2008.4 ± 0.7 [15]	2022	1^-	$1S_{1/2}$	3.94	$1.52e_q + 0.725e_Q$
B_s	5369.6 ± 2.4 [15]	5363	0^-	$1S_{1/2}$	3.91	0
B_s^*	5416.3 ± 3.3 [15]	5424	1^-	$1S_{1/2}$	3.91	$1.52e_q + 0.203e_Q$
B_{0_s}	not observed	5667	0^+	$2P_{1/2}$	4.47	0
B_{1_s}	not observed	5737	1^+	$2P_{1/2}$	4.47	$0.619e_q + 0.203e_Q$
B_{1_s}	5874 [16]	5718	1^+	$2P_{3/2}$	4.45	$1.93e_q + 0.101e_Q$
B_{2_s}	5886 [16]	5732	2^+	$2P_{3/2}$	4.45	$2.31e_q + 0.203e_Q$
B_s'	not observed	5887	0^-	$2S_{1/2}$	4.87	0
$B_s'^*$	not observed	6008	1^-	$2S_{1/2}$	4.87	$0.593e_q + 0.203e_Q$

5 Decays

We have looked at the electromagnetic and pionic transitions between mesons listed in Tables 1 and 2. The pionic transitions are calculated using the surface-coupling version of the chiral bag model [18]. In this model, a pion field carries the axial current outside the bag produced by the light (u or d) quark inside the bag. This makes the model chirally symmetric for massless u and d quarks and the interaction between the bag and the pion field is given by:

$$\mathcal{L}_{\mathrm{int}} = -\frac{\mathrm{i}}{2f_\pi}\overline{\psi}\gamma_5 \boldsymbol{\tau}\cdot\boldsymbol{\phi}\psi\Delta_s, \tag{26}$$

τ_i are the Pauli isospin matrices, and $\boldsymbol{\phi}$ an isovector representing the pion field. Δ_s is a covariant-surface delta function.

The calculation of transitions involving pions is then straightforward; some expressions for pionic transitions are listed below.

$$0^- \longrightarrow 1^-0^- \begin{cases} V_{fi} = \frac{-\mathrm{i}}{f_\pi}\sqrt{\frac{\pi}{3V\omega_{\boldsymbol{k}}}}P(R) \\ \quad \times \left(Y_1^{-1}(\hat{\boldsymbol{k}}) + Y_1^1(\hat{\boldsymbol{k}}) + Y_1^0(\hat{\boldsymbol{k}})\right) C_\pi \\ \Gamma(B' \longrightarrow B^*\pi) = \frac{1}{4\pi}\frac{k}{f_\pi^2}|P(R)C_\pi|^2 \end{cases} \tag{27}$$

$$0^- \longrightarrow 0^+0^- \begin{cases} V_{fi} = \frac{-1}{f_\pi}\sqrt{\frac{\pi}{V\omega_{\boldsymbol{k}}}}S(R)Y_0^0(\hat{\boldsymbol{k}})C_\pi \\ \Gamma(B' \longrightarrow B_0\pi) = \frac{1}{4\pi}\frac{k}{f_\pi^2}|S(R)C_\pi|^2 \end{cases} \tag{28}$$

$$2^+ \longrightarrow 0^-0^- \begin{cases} V_{fi} = -\frac{1}{f_\pi}\sqrt{\frac{2\pi}{5V\omega_{\boldsymbol{k}}}}D(R)Y_2^2(\hat{\boldsymbol{k}})C_\pi \\ \Gamma(B_2 \longrightarrow B\pi) = \frac{1}{10\pi}\frac{k}{f_\pi^2}|D(R)C_\pi|^2 \end{cases} \tag{29}$$

$$2^+ \longrightarrow 1^-0^- \begin{cases} V_{fi} = \frac{1}{f_\pi}\sqrt{\frac{2\pi}{5V\omega_{\boldsymbol{k}}}}D(R) \\ \quad \times \left(Y_2^2(\hat{\boldsymbol{k}}) - \frac{1}{\sqrt{2}}Y_2^1(\hat{\boldsymbol{k}})\right) C_\pi \\ \Gamma(B_2 \longrightarrow B^*\pi) = \frac{3}{20\pi}\frac{k}{f_\pi^2}|D(R)C_\pi|^2 \end{cases} \tag{30}$$

$$1^+ \longrightarrow 1^-0^- \begin{cases} V_{fi} = \frac{1}{f_\pi}\sqrt{\frac{\pi}{10V\omega_{\boldsymbol{k}}}}D(R)\left(\sqrt{6}Y_2^2(\hat{\boldsymbol{k}})\right. \\ \quad \left. - \sqrt{3}Y_2^1(\hat{\boldsymbol{k}}) + Y_2^0(\hat{\boldsymbol{k}})\right) C_\pi \\ \Gamma(B_1(P_{3/2}) \longrightarrow B^*\pi) = \frac{1}{4\pi}\frac{k}{f_\pi^2}|D(R)C_\pi|^2 \end{cases} \tag{31}$$

$$1^+ \longrightarrow 1^-0^- \begin{cases} V_{fi} = \frac{1}{f_\pi}\sqrt{\frac{\pi}{V\omega_{\boldsymbol{k}}}}S(R)Y_0^0(\hat{\boldsymbol{k}})C_\pi \\ \Gamma(B_1(P_{1/2}) \longrightarrow B^*\pi) \\ \quad = \frac{1}{4\pi}\frac{k}{f_\pi^2}|S(R)C_\pi|^2 \end{cases} \tag{32}$$

$$0^+ \longrightarrow 0^-0^- \begin{cases} V_{fi} = -\frac{1}{f_\pi}\sqrt{\frac{\pi}{V\omega_{\boldsymbol{k}}}}S(R)Y_0^0(\hat{\boldsymbol{k}})C_\pi \\ \Gamma(B_0 \longrightarrow B\pi) = \frac{1}{4\pi}\frac{k}{f_\pi^2}|S(R)C_\pi|^2 \end{cases} \tag{33}$$

$$1^- \longrightarrow 0^-0^- \begin{cases} V_{fi} = \frac{-\mathrm{i}}{f_\pi}\sqrt{\frac{\pi}{3V\omega_{\boldsymbol{k}}}}P(R)Y_1^1(\hat{\boldsymbol{k}})C_\pi \\ \Gamma(D^* \longrightarrow D\pi) \\ \quad = \frac{1}{12\pi}\frac{k}{f_\pi^2}|P(R)C_\pi|^2. \end{cases} \tag{34}$$

In these formulas,

$$S(R) \equiv R^2\left(f_\beta^*(R)g_\alpha(R) + g_\beta^*(R)f_\alpha(R)\right)j_0(kR) \quad \text{(S wave)} \tag{35}$$

$$P(R) \equiv R^2\left(f_\beta^*(R)g_\alpha(R) + g_\beta^*(R)f_\alpha(R)\right)j_1(kR) \quad \text{(P wave)} \tag{36}$$

$$D(R) \equiv R^2\left(f_\beta^*(R)g_\alpha(R) + g_\beta^*(R)f_\alpha(R)\right)j_2(kR) \quad \text{(D wave).} \tag{37}$$

The index $\alpha(\beta)$ refers to the initial (final) meson and

$$C_\pi \equiv \begin{cases} 1 & \text{for} \quad \pi^\pm \\ \frac{1}{\sqrt{2}} & \text{for} \quad \pi^0. \end{cases} \tag{38}$$

The above transition rates (27)–(34) have been numerically calculated and are listed in Table 3.

Table 3. Pion decays

$J_\alpha^{P\alpha} \longrightarrow J_\beta^{P\beta}\pi$	$\alpha \longrightarrow \beta\pi$	Theor (MeV)	$g_{\alpha\beta\pi}$
$0^- \longrightarrow 1^-\pi$	$B' \longrightarrow B^*\pi^+$	84.3	42.8
	$B' \longrightarrow B^*\pi^0$	42.2	30.1
$0^- \longrightarrow 0^+\pi$	$B' \longrightarrow B_0\pi^+$	45.3	23.0
	$B' \longrightarrow B_0\pi^0$	22.7	16.2
$2^+ \longrightarrow 1^-\pi$	$B_2 \longrightarrow B^*\pi^+$	9.17	55.8
	$B_2 \longrightarrow B^*\pi^0$	4.67	39.4
$2^+ \longrightarrow 0^-\pi$	$B_2^+ \longrightarrow B^0\pi^+$	9.74	43.5
	$B_2^0 \longrightarrow B^0\pi^0$	4.94	30.7
	$B_2^+ \longrightarrow B^+\pi^0$	4.98	30.7
	$B_2^0 \longrightarrow B^+\pi^-$	9.82	43.5
$1^+(P_{3/2}) \longrightarrow 1^-\pi$	$B_1 \longrightarrow B^*\pi^+$	13.3	72.8
	$B_1 \longrightarrow B^*\pi^0$	6.71	51.1
$1^+(P_{1/2}) \longrightarrow 1^-\pi$	$B_1 \longrightarrow B^*\pi^+$	92.7	27.1
	$B_1 \longrightarrow B^*\pi^0$	46.1	19.0
$0^+ \longrightarrow 0^-\pi$	$B_0^+ \longrightarrow B^0\pi^+$	93.7	28.5
	$B_0^0 \longrightarrow B^0\pi^0$	46.8	20.1
	$B_0^+ \longrightarrow B^+\pi^0$	46.9	20.1
	$B_0^0 \longrightarrow B^+\pi^-$	93.7	28.5
$1^- \longrightarrow 0^-\pi$	$D^{*+} \longrightarrow D^0\pi^+$	$6.01\ 10^{-2}$	17.1
	$D^{*+} \longrightarrow D^+\pi^0$	$2.72\ 10^{-2}$	12.1
	$D^{*0} \longrightarrow D^0\pi^0$	$3.88\ 10^{-2}$	12.1

In addition to the partial widths listed in Table 3, we have also calculated the coupling constants (on the right in Table 3), by using the following definition:

$$g_{\alpha\beta\pi} \equiv \sqrt{\frac{\Gamma(\alpha \longrightarrow \beta\pi)24\pi M_\alpha^2}{k^{2L+1}}} \tag{39}$$

where k is the pion momenta and M_α the mass of the decaying particle. The dimension of the couplings goes as $(\mathrm{GeV})^{-L+1}$, where L is the relative angular momentum between the decay products. Only $L = 1$ transitions, such as $1^- \longrightarrow 0^-\pi$ are then dimensionless by the definition (39).

It is also possible to calculate the coupling $g_{B^*B\pi}$; the B^* emits a virtual pion. This coupling has been calculated in the rest system of the heavy meson at zero recoil; the result is:

$$g_{B^*B\pi^\pm} = \sqrt{\frac{2}{9}}\frac{R}{f_\pi}|R^2\left(f_\beta^*(R)g_\alpha(R) + g_\beta^*(R)f_\alpha(R)\right)|M_{B^*} \tag{40}$$

$$g_{B^*B\pi^0} = \sqrt{\frac{1}{9}}\frac{R}{f_\pi}|R^2\left(f_\beta^*(R)g_\alpha(R) + g_\beta^*(R)f_\alpha(R)\right)|M_{B^*}. \tag{41}$$

Using the wave functions for the B^* and B meson, we obtain

$$g_{B^*B\pi^+} = 45.6, \tag{42}$$

$$g_{B^*B\pi^0} = 32.2. \tag{43}$$

Table 4. Photon decays

$J_\alpha^P \longrightarrow J_\beta^P\pi$	$\alpha \longrightarrow \beta\pi$	Theor (keV)
$0^- \longrightarrow 2^+ + 1^-$	$B^{**0} \longrightarrow B_2^0\gamma$	$2.62\ 10^{-3}$
	$B^{**+} \longrightarrow B_2^+\gamma$	$1.05\ 10^{-2}$
$0^- \longrightarrow 1^+ + 1^-$	$B^{**0} \longrightarrow B_1^0\gamma$	$1.77\ 10^{1}$
	$B^{**+} \longrightarrow B_1^+\gamma$	$7.07\ 10^{1}$
$0^- \longrightarrow 1^- + 1^-$	$B^{**0} \longrightarrow B^{*0}\gamma$	$1.20\ 10^{-1}$
	$B^{**+} \longrightarrow B^{*+}\gamma$	$7.89\ 10^{-1}$
$0^- \longrightarrow 0^- + 1^-$	$B^{**0} \longrightarrow B^0\gamma$	0
	$B^{**+} \longrightarrow B^+\gamma$	0
$2^+ \longrightarrow 1^+ + 1^-$	$B_2^0 \longrightarrow B_1^0\gamma$	$6.26\ 10^{-2}$
	$B_2^+ \longrightarrow B_1^+\gamma$	$2.50\ 10^{-3}$
$2^+ \longrightarrow 1^- + 1^-$	$B_2^0 \longrightarrow B^{*0}\gamma$	$6.76\ 10^{1}$
	$B_2^+ \longrightarrow B^{*+}\gamma$	$2.70\ 10^{2}$
$2^+ \longrightarrow 0^- + 1^-$	$B_2^0 \longrightarrow B^0\gamma$	4.08
	$B_2^+ \longrightarrow B^+\gamma$	$1.63\ 10^{1}$
$2^+ \longrightarrow 1^+ + 1^-$	$B_{s2}^0 \longrightarrow B_{s1}^0\gamma$	$3.38\ 10^{-4}$
$2^+ \longrightarrow 1^- + 1^-$	$B_{s2}^0 \longrightarrow B_s^{*0}\gamma$	$5.86\ 10^{1}$
$2^+ \longrightarrow 0^- + 1^-$	$B_{s2}^0 \longrightarrow B_s^0\gamma$	4.62
$1^+ \longrightarrow 1^- + 1^-$	$B_1^0 \longrightarrow B^{*0}\gamma$	$2.73\ 10^{1}$
	$B_1^+ \longrightarrow B^{*+}\gamma$	$1.09\ 10^{2}$
$1^+ \longrightarrow 0^- + 1^-$	$B_1^0 \longrightarrow B^0\gamma$	$4.10\ 10^{1}$
	$B_1^+ \longrightarrow B^+\gamma$	$1.64\ 10^{2}$
$1^+ \longrightarrow 1^- + 1^-$	$B_{s1}^0 \longrightarrow B_s^{*0}\gamma$	$2.56\ 10^{1}$
$1^+ \longrightarrow 0^- + 1^-$	$B_{s1}^0 \longrightarrow B_s^0\gamma$	$3.46\ 10^{1}$
$1^- \longrightarrow 0^- + 1^-$	$B^{*0} \longrightarrow B^0\gamma$	$6.41\ 10^{-2}$
	$B^{*+} \longrightarrow B^+\gamma$	$2.72\ 10^{-1}$
	$B_s^{*0} \longrightarrow B_s^0\gamma$	$5.10\ 10^{-2}$
	$D^{*0} \longrightarrow D^0\gamma$	7.18
	$D^{*+} \longrightarrow D^+\gamma$	1.73

The coupling of photons to the mesonic states are done straightforwardly by using the interaction Lagrangian:

$$\mathcal{L}_{\mathrm{int}} = e_q e\overline{\psi}\boldsymbol{\gamma}\cdot\boldsymbol{A}\psi \tag{44}$$

Some expressions for electromagnetic transitions are listed below:

$$0^- \longrightarrow 2^+1^- \left\{\Gamma = \ \tfrac{24}{5}\alpha e_q^2\omega_{\boldsymbol{k}}\left|\int \mathrm{d}x j_2(F+G)\right|^2 \right. \tag{45}$$

$$0^- \longrightarrow 1^+1^- \begin{cases} \Gamma = \ \tfrac{8}{3}\alpha e_q^2\omega_{\boldsymbol{k}}\left(\ \tfrac{1}{5}\left|\int \mathrm{d}x j_2(F+G)\right|^2\right. \\ \qquad + \left|\int \mathrm{d}x(Fj_2 - Gj_0)\right|^2 \\ \qquad \left. + \tfrac{1}{3}\left|\int \mathrm{d}x(Gj_2 + Gj_0)\right|^2\right) \end{cases} \tag{46}$$

$$0^- \longrightarrow 1^-1^- \left\{\Gamma = \ \tfrac{24}{5}\alpha e_q^2\omega_{\boldsymbol{k}}\left|\int \mathrm{d}x j_1(F+G)\right|^2 \right. \tag{47}$$

$$0^- \longrightarrow 0^-1^- \left\{\Gamma = \ 0 \right. \tag{48}$$

Table 5. Comparison of theoretical and experimental results

	Theoretical				Experimental
	[19](MeV)	[20](keV)	[21](keV)	Our work	[15](keV)
$\Gamma(B_2 \longrightarrow B^*\pi)$	11	–	–	13.8MeV	–
$\Gamma(B_2 \longrightarrow B\pi)$	10	–	–	14.7MeV	–
$\Gamma(B_1 \longrightarrow B^*\pi)$	14	–	–	20.0MeV	–
$\Gamma(B^{*+} \longrightarrow B\gamma)$	–	–	0.38 ± 0.06	0.272keV	–
$\Gamma(B^{*0} \longrightarrow B^0\gamma)$	–	–	0.13 ± 0.03	$6.41\ 10^{-2}$keV	–
$\Gamma(B_s^* \longrightarrow B_s\gamma)$	–	–	0.22 ± 0.04	$5.10\ 10^{-2}$keV	–
$\Gamma(D^{*+} \longrightarrow D^0\pi^+)$	–	69.1	–	60.1keV	< 91
$\Gamma(D^{*+} \longrightarrow D^+\pi^0)$	–	32.1	–	27.2keV	< 43
$\Gamma(D^{*0} \longrightarrow D^0\pi^0)$	–	46.0	–	38.8keV	< 85
$\Gamma(D^{*+} \longrightarrow D^+\gamma)$	–	0.919	0.23 ± 0.1	1.72keV	< 4.2
$\Gamma(D^{*0} \longrightarrow D^0\gamma)$	–	23.5	12.9 ± 2	7.18keV	< 54

$$2^+ \longrightarrow 1^+1^- \begin{cases} \Gamma = & \frac{2}{375}\alpha e_q^2 \omega_{\boldsymbol{k}} \left(\frac{87}{4} \left| \int \mathrm{d}x j_1 (F+G) \right|^2 \right. \\ & +52 \left| \int \mathrm{d}x (G j_3 + G j_1) \right|^2 \\ & +2 \left| \int \mathrm{d}x (G j_3 - F j_1) \right|^2 \\ & +27 \left| \int \mathrm{d}x (F j_3 - G j_1) \right|^2 \\ & +27 \left| \int \mathrm{d}x (F j_3 + F j_1) \right|^2 \\ & \left. +\frac{3501}{7} \left| \int \mathrm{d}x j_3 (F+G) \right|^2 \right) \end{cases} \quad (49)$$

$$2^+ \longrightarrow 1^-1^- \begin{cases} \Gamma = & \frac{4}{3}\alpha e_q^2 \omega_{\boldsymbol{k}} \left(\frac{11}{10} \left| \int \mathrm{d}x j_2 (F+G) \right|^2 \right. \\ & + \left| \int \mathrm{d}x (G j_2 - F j_0) \right|^2 \\ & \left. +\frac{1}{3} \left| \int \mathrm{d}x (F j_2 + F j_0) \right|^2 \right) \end{cases} \quad (50)$$

$$2^+ \longrightarrow 0^-1^- \left\{ \Gamma = \quad \frac{6}{5}\alpha e_q^2 \omega_{\boldsymbol{k}} \left| \int \mathrm{d}x j_2 (F+G) \right|^2 \right. \quad (51)$$

$$1^+ \longrightarrow 1^-1^- \begin{cases} \Gamma = & \frac{2}{9}\alpha e_q^2 \omega_{\boldsymbol{k}} \left(13 \left| \int \mathrm{d}x j_2 (F+G) \right|^2 \right. \\ & +\frac{2}{3} \left| \int \mathrm{d}x (F j_2 + F j_0) \right|^2 \\ & \left. +2 \left| \int \mathrm{d}x (G j_2 - F j_0) \right|^2 \right) \end{cases} \quad (52)$$

$$1^+ \longrightarrow 0^-1^- \begin{cases} \Gamma = & \frac{8}{9}\alpha e_q^2 \omega_{\boldsymbol{k}} \left(-\frac{1}{4} \left| \int \mathrm{d}x j_2 (F+G) \right|^2 \right. \\ & +\frac{1}{3} \left| \int \mathrm{d}x (F j_2 + F j_0) \right|^2 \\ & \left. + \left| \int \mathrm{d}x (G j_2 - F j_0) \right|^2 \right) \end{cases} \quad (53)$$

$$1^- \longrightarrow 0^-1^- \left\{ \Gamma = \quad \frac{4}{3}\alpha e_q^2 \omega_{\boldsymbol{k}} \left| \int \mathrm{d}x j_1 (F+G) \right|^2 , \right. \quad (54)$$

where we have defined:

$$F \equiv x^2 f_\beta(x)^* g_\alpha(x), \quad (55)$$

$$G \equiv x^2 g_\beta(x)^* f_\alpha(x), \quad (56)$$

$$j_1 \equiv j_1(\omega_{\boldsymbol{k}} x). \quad (57)$$

The numerical values for the above expressions are shown in Table 4. The transitions in Table 4 are very suppressed in comparison with those listed in Table 3. This is, of course, expected; the smaller phase space for pion decays is compensated for by the much stronger pion coupling (relative to the electromagnetic coupling).

6 Comparison with theoretical and experimental results

We have calculated a lot of partial widths for different particles, listed in Tables 3 and 4. To date, very little is known on the experimental front, but there are a lot of theoretical predictions. We will compare our results with the known experimental results, and some of the theoretical results; as we shall see, there is no conflict between our predictions and the experimental information.

In Table 5, we have listed some theoretical and experimental results. For the experimental limits, we have assumed that the widths of D^{*0} have the same upper limit as the widths of $D^{*\pm}$. It may not be clear from Table 5, but the theoretical predictions vary a lot. In [22], there is a summary of theoretical estimates. For the particular decay $D^{*+} \longrightarrow D^0\pi^+$ that determines the coupling constant $g_{D^*D\pi}$, the predicted rates vary from 10keV (QCD sum rules) to more than 100keV (quark model + chiral HQET). We obtained $\Gamma(D^{*+} \longrightarrow D^0\pi^+) = 60.1$keV, which is close to the value 61–78 keV from P. Cho and H. Georgi [23], who make calculations with chiral HQET. The value of the coupling $g_{B^*B\pi^+}$ vary from $g_{B^*B\pi^+} = 15 \pm 4$ (QCD sum rules) to $g_{B^*B\pi^+} = 64$ (quark model + chiral HQET); we found $g_{B^*B\pi^+} = 45.6$.

We have calculated most, but not all, decay modes for the excited states. The $\pi\pi$ modes are missing. As we believe that these modes are less important than the emission of single pions in the decays, we still can give approximate values of the decay widths; these are:

$$2S_{1/2} \ : \quad \Gamma(B') \simeq 195\text{MeV} \quad (58)$$

$$2P_{3/2} \ : \quad \Gamma(B_2) \simeq 29\text{MeV} \qquad \Gamma(B_1) \simeq 20\text{MeV} \quad (59)$$

$$2P_{1/2} \ : \quad \Gamma(B_1) \simeq 139\text{MeV} \qquad \Gamma(B_0) \simeq 141\text{MeV} \quad (60)$$

$$1S_{1/2} \ : \quad \Gamma(D^{*+}) \simeq 89\text{keV} \qquad \Gamma(D^{*0}) \simeq 46\text{keV} \quad (61)$$

The $P_{1/2}$ states are naturally much wider than the $P_{3/2}$ states, because they decay only through an S wave, whereas the $P_{3/2}$ states decay through a D wave. The full widths of the P states indicated by a preliminary experiment [24] are $\Gamma(B(P_{3/2})) \simeq 20$ MeV and $\Gamma(B(P_{1/2})) \simeq$

Table 6. Comparison of CLEO data and our predictions

	CLEO	Our calculations
$B_r(D^{*+} \longrightarrow D^+\gamma)$	$(1.68 \pm 0.51)\%$	1.94%
$B_r(D^{*+} \longrightarrow D^+\pi^0)$	$(30.73 \pm 0.63)\%$	30.55%
$B_r(D^{*+} \longrightarrow D^+\pi^+)$	$(67.59 \pm 0.70)\%$	67.51%

150 MeV. This is, as we see, in good agreement with our results. Since the $P_{1/2}$ states are so broad, they are very hard to reconstruct from the experimental results, and so far there has not been any really precise measurement of their masses.

The CLEO report [25] contains the best measurement of the D^{*+} branching fractions, a large improvement over what can be found in the Particle Data Book [15]. Since we have calculated the width of the D^{*+} meson (in (61), it is easy to calculate the branching ratios. The results are shown in Table 6 together with the CLEO results. Our results are clearly in good agreement with the experimental data. We recognize, however, that branching ratios are one thing, and particular decay widths another. We get the correct ratio between pionic and electromagnetic decays. As the coupling of the electromagnetic field to the quarks is simple, we naturally have some confidence in the calculated electromagnetic transition rates. Therefore we believe that our calculated pionic rates cannot be too far off from what will be measured in the future.

References

1. Nathan Isgur, Mark B. Wise, Phys. Lett. B **232**, 113 (1989)
2. Nathan Isgur, Mark B. Wise, Phys. Lett. B **237**, 527 (1990)
3. H. Georgi, Phys. Lett. B **240**, 447 (1990)
4. E. Eichten, B. Hill, Phys. Lett. B **234**, 511 (1990)
5. E. Eichten, B. Hill, Phys. Lett. B **243**, 259 (1990)
6. M. Neubert, Phys. Rep. **245**, 259 (1994)
7. Walter Wilcox, O.V. Maxwell, Kimball A. Milton, Phys. Rev. D **31**, 1081 (1985)
8. H. Hogaasen, M. Sadzikowski, Z. Phys. C **64**, 427 (1994)
9. M. Sadzikowski, K. Zalewski, Z. Phys. C **59**, 677 (1993)
10. P.N. Bogolioubov, Ann. Inst. Henri Poincaré **VIII**, 163 (1968)
11. A. Chodos, R.L. Jaffe, K. Johnson, C.B. Thorn, V.F. Weisskopf, Phys. Rev. D **9**, 3471 (1974)
12. H. Hogaasen, J.M. Richard, P. Sorba, Phys. Lett. B **119**, 272 (1982)
13. Kimball A. Milton, Lester L. DeRaad, Jr., Julian Schwinger, Ann. of Phys. **115**, 388 (1978)
14. Dale Izatt, Carleton Detar, Mark Stephenson Nucl. Phys. B **199**, 269 (1982)
15. C. Cisco, et al., Euro. Phys. J. C **3**, 1 (1998)
16. OPAL Collaboration, R. Akers, et al., Z. Phys. C **66**, 19 (1995)
17. C. Weiser, Talk given at the XXVII International Conference on High Energy Physics, Warsaw, 25–31 July 1996
18. A.W. Thomas, Adv. Nuc. Phys. **13**, 1 (1983)
19. Estia J. Eichten, Christopher T. Hill, Chris Quigg, Phys. Rev. Lett. **71**, 4116 (1993)
20. Patric J. O'Donnel, Q.P. Xu, Phys. Lett. B **336**, 113 (1994)
21. Shi-Lin Zhu, W-Y.P. Hwang, Ze-sen Yang, Mod. Phys. Lett A **12**, 3027 (1997) see also: Yuan-Ben Dai, Shi-Lin Zhu, Phys. Rev. D **58**, 074009 (1998); Yuan-Ben Dai, Shi-Lin Zhu, Euro. Phys. J. C **6**, 307 (1999); Shi-Lin Zhu and Yuan-Ben Dai, Phys. Rev. D **58**, 094033 (1998); Shi-Lin Zhu, Yuan-Ben Dai, [hep-ph/9810243]
22. V.M. Belyaev, V.M. Braun, A. Khodjamirian, R. Rückl, Phys. Rev D **51**, 6177 (1995)
23. Peter Cho, Howard Georgi, Phys. Lett. B **296**, 408 (1992)
24. DELPHI Collaboration, P. Abreu, et al., Phys. Lett. B **345**, 598 (1995)
25. J. Bartelt, et al., Phys. Rev. Lett. **80**, 3919 (1998)